DEFECT DETECTION OF GFRP LAMINATES BY BARKER CODEDMODULATION EXCITATION INFRARED THERMAL IMAGING

by

Qing-Ju TANG[a,*], Ling RAN[a], Ze-Shen QU[a], Chi-Wu BU[b]

[a] School of Mechanical Engineering, Heilongjiang University of Science and Technology, Harbin 150022, China

[b]College of Light Industry, Harbin University of Commerce, Harbin 150028, China

During the preparation and service of GFRP laminates, due to the influence of manufacturing process, it is easy to produce debonding defect. This paper expounds the basic principle and test process of infrared nondestructive testing, which using the barker code modulation of the thermal wave to identify the GFRP laminate debonding defect. Through the establishment of infrared thermal imaging testing system, this paper studies its detection effect on defects with different diameter, depth and diameter-to-depth ratio, processes the image sequence by using principal component analysis (PCA) and discrete Fourier transform (DFT) algorithms, and finally calculates and compares the processed signal-to-noise ratio (SNR). The results show that Barker code modulated thermal wave infrared detection can detect the debonding defects of GFRP laminates. Among them, the detection effect of 13-bit Barker coded modulation excitation is better, and the image processed by DFT has better recognition effect.

Keywords: *GFRP laminates, Barker coded modulation excitation, image sequence processing*

Introduction

GFRP has the advantages of high strength, good corrosion resistance, impact resistance, fatigue resistance and wave absorption performance, which is widely used in machinery, aerospace, shipbuilding, construction and energy industries. At present, GFRP laminates still have the advantages of high strength, small specific gravity and corrosion resistance in the aerospace field of aircraft manufacturing, which were used in the radome and inlet of aircraft and the leading edge of the wing [1,2]. However, due to the particularity of the structure and preparation process, it is easy to produce debonding defects in the manufacturing and service process of GFRP laminates [3], and the internal defect state cannot

* Corresponding author; e-mail: tangqingju@126.com

be judged by naked eyes. Therefore, it is necessary to detect GFRP laminates.

As an emerging non-destructive testing technology, infrared thermal imaging NDT technology Including incentives, data collection and data processing system, which had been widely applied in the detection of defects such as debonding, crack, rust, fatigue and damage in metal, non-metal and composite materials [4,5].Compared with traditional nondestructive testing techniques such as ray, ultrasonic, magnetic powder, penetration and eddy current, it has many advantages such as non-contact, large single test area, high efficiency, safety, intuitive test results and simple operation [6,7].

Both linear frequency modulation thermal wave imaging and two-phase coded thermal wave imaging belong to coded infrared thermal imaging. The latter refers to the thermal wave modulated by two-phase code as a thermal excitation source[8], among which barker code [9,11] is the most important two-phase coding in radar system. Barker code, a very ideal pulse compression coding, is a group of binary sequence coding group with specific permutation and non-periodicity proposed by R. H. Barker in 1953, which is applied to the infrared thermal wave nondestructive testing technology to modulate the excitation signal of the tested sample. The excitation source encoded by Barker code can concentrate energy, improve the detection ability of surface and subsurface defects and improve the image signal-to-noise ratio (SNR).

Thermal waves with Barker coded excitation detection principle

The barker code is a set of specific binary sequences, which can make the ratio of the peak value of the pulse compression signal to the maximum sidelobe N:1, N is the length of the code, it has the characteristics of small side lobe amplitude and large main and side lobe ratio, and has ideal autocorrelation characteristics. At present, there are only 7 different lengths and 9 categories of Known Barker codes, which code lengths of 2, 3, 4, 5, 7, 11 and 13 bits respectively. There are two groups of codes when N=2 and N=4, and Barker codes of odd length with N>13 do not exist [12]. The main peak of barker code autocorrelation function is equal to the code length, and the side lobe value of autocorrelation sequence always jumps between 0,1 and -1, which is a very ideal pulse compression coding.

The complex expressions of general phase coded signals can be written as

$$s(t) = a(t)e^{j\varphi(t)}e^{j2\pi f_0 t} \tag{1}$$

Then the complex envelope of its signal is given as

$$u(t) = a(t)e^{j\varphi(t)} \tag{2}$$

where f_0 is carrier frequency, $\varphi(t)$ is phase modulation function, for two-phase coded signals, and $\varphi(t)$ may be 0 or π.

Its aperiodic autocorrelation function is defined as：

$$R(m) = \sum_{k=0}^{N-1-|m|} c_k\, c_{k+m} = \begin{cases} N, & m = 0 \\ 0\ or \pm 1, & m \neq 0 \end{cases} \tag{3}$$

The principle of barker code modulated thermal wave nondestructive testing can be summarized as follows: thermal wave that halogen lamp signal is coded modulation generate temperature field on the surface of the object to be measured, then temperature difference will occur between defect and non-defect areas. Infrared thermal imager is used to collect temperature signals on the surface of the specimen in excitation process, and the signals are

transmitted to the computer.

Barker coded modulation infrared thermal imaging test system

Test equipment

The experimental system is mainly composed of excitation system, acquisition system and image sequence processing. The infrared thermal imager model is FLIR655SC, pixel resolution is 640×480, thermal sensitivity is 0.03℃, peak power of a single halogen lamp is 1000W, and data acquisition card model is Ni-USB6259BNC.

Sample preparation

GFRP laminates with the size of 160mm×140mm×5mm were prepared. Blind holes were drilled to simulate debonding defects of different diameters and depths. Single-layer laying was adopted for the specimens, and the influence of layering method on the experiment was ignored. Tab. 1 shows the defect sizes of GFRP laminates.

Table 1. Debonding defect sizes of sample

Row \ Column	1	2	3	4	5
1	DA=2	DA=2	DA=2	DA=2	DA=2
	DL=2.5	DL=3	DL=3.5	DL=4	DL=4.5
2	DA=4	DA=4	DA=4	DA=4	DA=4
	DL=2.5	DL=3	DL=3.5	DL=4	DL=4.5
3	DA=6	DA=6	DA=6	DA=6	DA=6
	DL=2.5	DL=3	DL=3.5	DL=4	DL=4.5
4	DA=8	DA=8	DA=8	DA=8	DA=8
	DL=2.5	DL=3	DL=3.5	DL=4	DL=4.5
5	DA=10	DA=10	DA=10	DA=10	DA=10
	DL=2.5	DL=3	DL=3.5	DL=4	DL=4.5

Where: DA is Defect diameter, mm; DL is Defect depth, mm

Experimental parameters

The 13-bit Barker code was used to modulate the pulse compression thermal wave, and the halogen lamp power was set to 1000W and scanning period to 30s to apply thermal excitation to the specimen. Set the sampling frequency of infrared thermal imager to 20Hz and acquisition time to 30s for image sequence collection.

Test results and analysis

Barker code modulated thermal wave excitation was applied to the specimen, and the original heat maps at different times were shown in Fig.1.

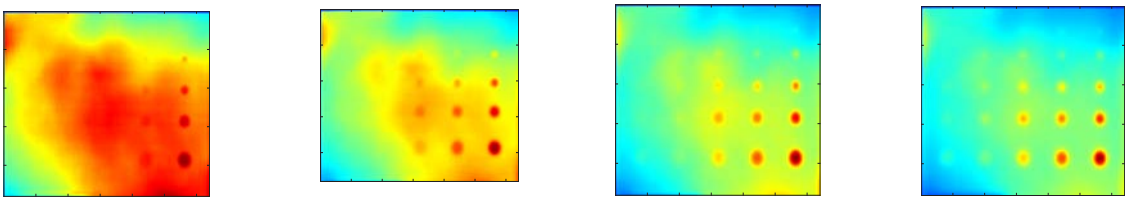

a) 5s **b) 9s** **c) 15s** **d) 20s**

Figure 1. Original heat maps at different times

As shown in Fig.1, through applying barker code modulated thermal excitation to the specimen, the defects in the specimen surface began to stand out at 5s after the sub-pulse compression thermal wave excitation of the first group. After the second group of short pulse compression thermal wave excitation9s, the shape and size of the defect are more obvious, but the transverse noise has a great influence. At the end of the modulation thermal wave excitation15s, the defect characteristics are clear and obvious compared with the previous moments. At 20s, the overall temperature of the specimen surface began to decrease, and after the thermal equilibrium stage, the defects in the specimen were basically all revealed. In general, barker code modulation thermal wave can realize the detection of debonding defects.

Theinfluence of defect geometry characteristics on surface temperature difference

As shown in Fig.2, the variation trend of surface temperature difference curve is basically consistent with that of barker code modulated heat flow. Fig.2 (a) shows that at the same defect depth, the larger the debonding diameter is, the more heat accumulated at the defect, and the larger the surface temperature difference is, then the easier the defect is to be detected.According to Fig.2 (b), when the defect diameter is same, the deeper of debonding defect depth is, the greater of surface temperature difference is, and then the defect is easy to be identified. Fig.2 (c) shows that different diameter-to-depth ratios also have a certain influence on the surface temperature difference. The larger of diameter-to-depth ratio is, the larger surface temperature difference is, and then the easier of existing defect is to be detected.

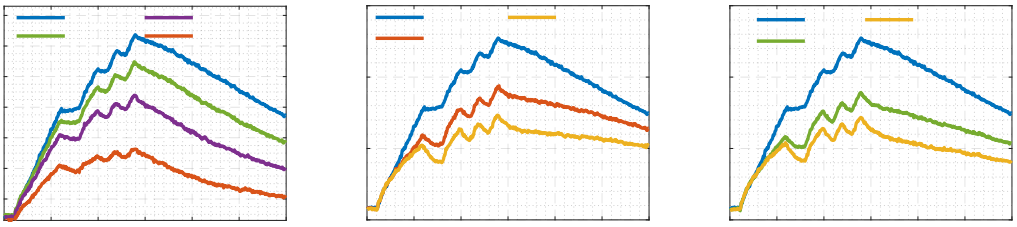

a) Different diametersb) Different depths c) Different diameter-to-depth ratio

Figure 2. Influence of geometric features on surface temperature difference

Image sequence processing

In the process of image acquisition, it will inevitably be affected by many factors, such as uneven heating, inconsistent material surface emissivity, ambient noise and performance of infrared thermal imager, so that the uneven surface temperature distribution in the image, large surface noise, and great influence on the detection effect. Image sequence processing to further dealt with recorded by infrared thermal imager to collect the component surface temperature field, and the processed results for display in the form of image, improve the SNR of infrared image, increase the defect contrast, thereby increasing the degree of visibility of defects, the detection of defects and defect geometric feature recognition.

Principal component analysis (PCA)

Principal component analysis (PCA)[13] is a method of dimensionality reduction of data in mathematics. Firstly, a set of arbitrary orthogonal basis Spaces with p principal eigenvectors identical to the principal molecular weight space are determined, and then the corresponding principal components were obtained after processing. The basic principle is as follows: N-dimensional observable random vector is set for sample evaluation. And based on standardized data processing, the general model of principal component analysis is:

$$\begin{Bmatrix} \mathrm{Z_1} = \mathrm{a_{11}X_1} + \mathrm{a_{12}X_2} + \cdots + \mathrm{a_{1p}X_p} \\ \mathrm{Z_2} = \mathrm{a_{21}X_1} + \mathrm{a_{22}X_2} + \cdots + \mathrm{a_{2p}X_p} \\ \vdots \\ \mathrm{Z_n} = \mathrm{a_{n1}X_1} + \mathrm{a_{n2}X_2} + \cdots + \mathrm{a_{np}X_p} \end{Bmatrix} \tag{4}$$

where $Z_1, Z_2, \ldots, Z_n$ are the first principal component, the second principal component…, the nth principal component, $X_1, X_2, \ldots, X_n$ are the common factor.

If the eigenvalue of the correlation coefficient matrix of X be λ, then the cumulative contribution rate k of the principal component can be expressed as:

$$k = \frac{\sum_{i=1}^{p} \lambda_i}{\sum_{i=1}^{n} \lambda_i} \tag{5}$$

Therefore, the greater the cumulative contribution rate is, the less information is lost. It is generally believed that when the sum of the variances of n principal components accounts for more than 85% of the total variance, the vast majority of information of the original factor x is basically retained.

Discrete Fourier transform (DFT)

Discrete Fourier transform (DFT)[14] analyzed the signal from the perspective of frequency domain. The signal was converted from the original time domain to the frequency domain, and its application in the image meant that the signal corresponding to each pixel point was changed. This implies that

$$F_n = \sum_{k=0}^{N-1} T(k) e^{-j2\pi nk/N} = R_n + jI_n \tag{6}$$

where $T(k)$ is the temperature value at pixel (x, y) in the infrared heat map of frame k, R_n, I_n are respectively the real and imaginary parts of the transformed complex number, and n is the serial number of discrete frequency.

And then, the amplitude and phase values at frequency N are respectively:

$$A(n) = \sqrt{{R_n}^2 + {I_n}^2} \tag{7}$$

$$\varphi(n) = arctan(I_n / R_n) \tag{8}$$

Algorithm evaluation

In order to compare the effects of different image processing algorithms and parameters, it is necessary to unify the evaluation criteria of image processing.

$$c = \frac{c_0 - c_{min}}{cmin_{\ max}} \tag{9}$$

where c is the normalized processing value, c_0 is the Raw data, c_{max} is the maximum ofc_0, and c_{min} is the minimum of c_0.

In order to meet the comparability of detection, a square feature set domain was

defined in the central position of the defect, and also defined another one in the defect-free region. All pixel feature values in the region were analyzed and their signal-to-noise ratio (SNR) was calculated. The larger the SNR is, the smaller the noise effect is, and then the better the defect detection effect is.

$$SNR = \frac{\overline{T} - \overline{t}}{\sigma} \tag{10}$$

where $\overline{T}$ is the mean value of eigenvalue in defect area, $\overline{t}$ is the mean value of eigenvalue in defect free area, and σ is the standard deviation of eigenvalue in defect free area.

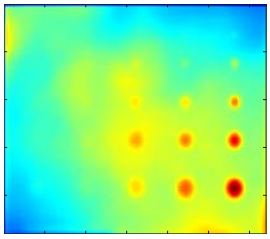

Figure 3. SNR reference area

GFRP specimens were tested and studied according to the test parameters. The obtained test data were processed by principal component analysis and Fourier transform method, and the image with the maximum signal-to-noise ratio was selected as the effect diagram after normalization, as shown in the figure below.

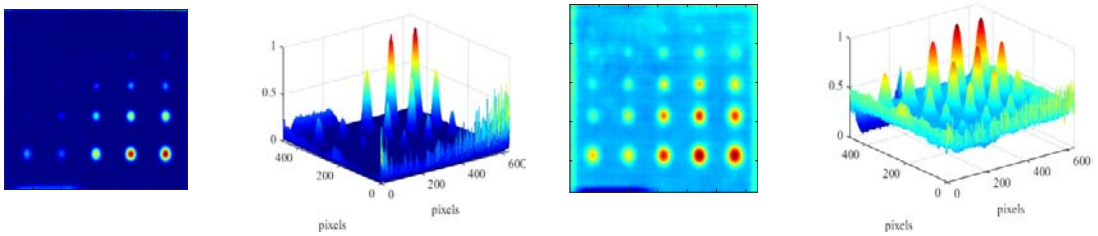

a) PC1 in2-D **b) PC1in 3-D** **c) PC2 in 2-D** **d) PC2 in 3-D**

Figure 4. Processing diagram of PCA

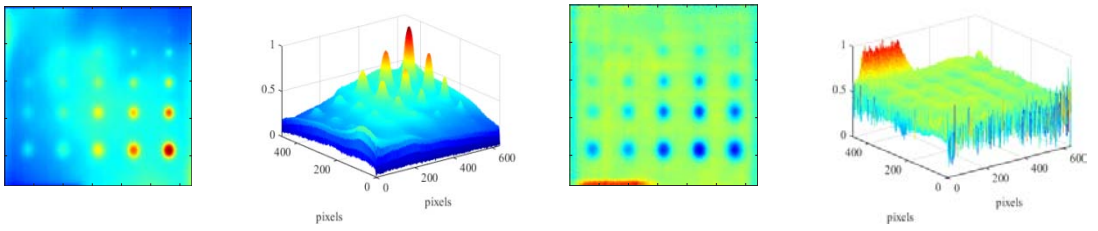

a) 2-D amplitude **b) 3-D amplitude** **a) 2-D phase diagram** **b) 3-D phase diagram**

Figure 5. Processing diagram of DFT

As shown in Fig.4 and Fig.5, the different effect image obtained after the same group of test data is processed by different image algorithms. Normalized processing and SNR parameters are used to evaluate the processing effect of PCA and DFT methods on experimental data.

The research shows that: the original image after DFT method and treatment effect is good, defect characteristics and clarity is better also, the contrast between defect area and

non-defect area difference is large. But the noise is reduced and the overall temperature field is evenly distributed after the image processed by PCA. It can be seen from the two-dimensional diagram that the image display of the processed defects is clearer and the geometric features of the defects are more obvious. From the three dimensional image, the larger the defect diameter and the deeper the defect depth, the more obvious the characteristics of debonding defect are.

The SNR of the images processed by both PCA and DFT was calculated, the SNR result under different diameters was shown in Fig.6.

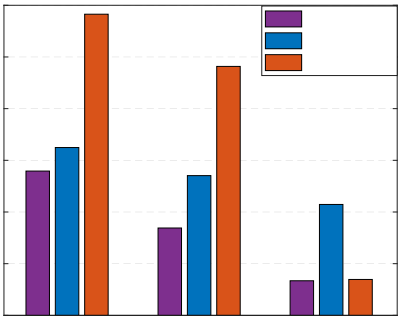

Figure 6.Calculation of SNR

It can be seen from Fig.6 that these two image sequence processing algorithms suppress noise to varying degrees, realize further image processing and facilitate defect detection and recognition. According to the calculation results of SNR, the image processed by DFT has higher SNR and better image quality.

Acknowledgment

This project is supported by National Natural Science Foundation of China (Grant No. 51775175),Heilongjiang Provincial Undergraduate University Funded Project of Basic Scientific Research Business Fee(Grant No. 2020-KYYWF-0696), and Heilongjiang Province Natural Science Fund (Grant No. LH2021E088).

Conclusion

In order to detect the debonding defects in GFRP laminates, this paper proposes a Barker coded modulation excitation. By building a barker code modulation heat source excitation system and using infrared thermal imager for acquisition, the original heat map sequence is finally acquired. Aiming at the problem of noise interference in original image, Both PCA and DFT were used to suppress noise in processing the original heat map sequence. it can be seen that the image processed by DFT has a higher SNR by calculating the SNR result, which can effectively extract the surface defect information of GFRP specimen test image.

Nomenclature

$\overline{T}$- mean value of eigenvalue, [℃]

$\overline{t}$-mean value of eigenvalue, [℃]

σ-standard deviation of eigenvalue, [-]

SNR-signal to noise ratio, [db]

References

[1] Lapina, O. B., *et al*.,Multinuclear NMR Study of Silica Fiberglass Modified with Zirconia, *Solid State Nuclear Magnetic Reso-nance*, 39 (2011), 3-4, pp. 47-57

[2] Gao, Y. L.,*et al*., Research Progress of High Performance Glass Fiber, *Shandong Chemical Industry*,49 (2020),5, pp. 78-79

[3] Wang, Y.,*et al*., Infrared Thermal Wave Detection of Delamination Defects in Glass Fiber Composites, *Nondestructive testing*, 32 (2010), 11, pp. 55-58

[4] Zhang, W.,*et al*., Infrared Thermal Wave Nondestructive Technology on the Defect in the Shell of Solid Rocket Motor, *Proceedings of SPIE-The International Society for Optical Engineering*, 7 (2010), 6, pp. 30-34

[5] Yan, Y. Q., *et al*., Step Thermal Excitation Infrared Thermal Wave Nondestructive Testing for Wind Turbine Blades,*2018 Far East NDT New Technology Forum*, (2018),pp. 442-449

[6] Liu, Y. T., *et al*.,The Development History, Present Situation and Trend of Infrared Thermal Imaging Nondestructive Testing Technology, *Nondestructive testing*, 39 (2017), 8,pp. 63-70

[7] Guo, W., *et al*.,Research Status and Development of Active Infrared Thermography Nondestructive Testing,*Nondestructive testing*, 38 (2016),4, pp. 58-62

[8] Shi, Q. Z., *et al*., Barker Code Excitation Infrared Thermal Imaging Detection of CFRP Laminates, in: *2018 Far East NDT New Technology Forum Proceedings, Far East Forum on New Technology of Nondestructive Testing*, 2018, pp. 470-475

[9] Ghali, V. S., *et al*., Barker Coded Thermal Wave Imaging for Defect Detection in Carbon Fibre-reinforced Plastics, *Insight-Non-Destructive Testing and Condition Monitoring*, 53 (2011), 53, pp. 621-624

[10] Dua, G., *et al*., Applications of Barker Coded Infrared Imaging Method for Characterization of Glass Fibre Reinforced Plastic Materials, *Electronics Letters*, 49 (2013), 17, pp. 1071-1073

[11] Mulaveesala, R., *et al*., Complementary Coded Thermal Wave Imaging Scheme for Thermal Non-destructive Testing and Evaluation, *Quantitative Infrared Thermography Journal*, 14 (2017), 1, pp. 44-53

[12] Storer, J. E., *et al*., Optimum Finite Code Groups, *Proc Ire*, 46 (1958), pp. 1649

[13] Sun, Q. L., *et al*., Image Segmentation Method Based on Principal Component Analysis, *Journal of Taiyuan University of Technology*, 49 (2018), 05, pp. 759-764

[14] Ma, Y. H., *et al*., Discrete Fourier Transform and its Application, *Chinese modern educational equipment*, 13(2015), pp. 56-58

Paper submitted: August 7, 2022
Paper revised: November 11, 2022
Paper accepted: November 22, 2022